mhFLIM: Resolution of heterogeneous fluorescence decays in widefield lifetime microscopy

S. Schlachter [1], A.D. Elder[1], A. Esposito[1], G.S. Kaminski[1], J.H. Frank[2], L.K. van Geest[3], and C.F. Kaminski[1,4]

[1]*Department of Chemical Engineering and Biotechnology, University of Cambridge, Pembroke St, Cambridge, CB2 1RA, U.K.*
[2]*Combustion Research Facility, Sandia National Laboratories, Livermore, CA 94551-0969*
[3]*Lambert Instruments Inc., 9301 ZP Roden, The Netherlands*
[4]*SAOT School of Advanced Optical Technologies, Max-Planck-Research Group, Division III University of Erlangen-Nuremberg, Günther-Scharowsky-Str. 1D-91058 Erlangen, Germany*

Corresponding authors: ss678@cam.ac.uk , cfk23@cam.ac.uk

http://laser.ceb.cam.ac.uk

Abstract: Frequency-domain fluorescence lifetime imaging microscopy (FD-FLIM) is a fast and accurate way of measuring fluorescence lifetimes in widefield microscopy. However, the resolution of multiple exponential fluorescence decays has remained beyond the reach of most practical FD-FLIM systems. In this paper we describe the implementation of FD-FLIM using a 40MHz pulse train derived from a supercontinuum source for excitation. The technique, which we term multi-harmonic FLIM (mhFLIM), makes it possible to accurately resolve biexponential decays of fluorophores without any *a priori* information. The system's performance is demonstrated using a mixture of spectrally similar dyes of known composition and also on a multiply-labeled biological sample. The results are compared to those obtained from time correlated single photon counting (TCSPC) microscopy and a good level of agreement is achieved. We also demonstrate the first practical application of an algorithm derived by G. Weber [1] for analysing mhFLIM data. Because it does not require nonlinear minimisation, it offers potential for realtime analysis during acquisition.

OCIS codes: (170.3650) Lifetime-based sensing; (180.2520) Fluorescence microscopy.

References and links

1. G. Weber, "Resolution of the fluorescence lifetimes in a heterogeneous system by phase and modulation measurements," J. Phys. Chem. **85**, 949–953 (1981).
2. S. M. Matthews, A. D. Elder, K. Yunus, C. F. Kaminski, C. M. Brennan, and A. C. Fisher, "Quantitative kinetic analysis in a microfluidic device using frequency-domain fluorescence lifetime imaging," Anal. Chem. **79**, 4101–4109 (2007).
3. H. J. Lin, P. Herman, and J. R. Lakowicz, "Fluorescence lifetime-resolved pH imaging of living cells," Cytometry Part A **52A**, 77–89 (2003).
4. X. W. Dai, Z. L. Yue, M. E. Eccleston, J. Swartling, N. K. H. Slater, and C. F. Kaminski, "Fluorescence intensity and lifetime imaging of free and micellar-encapsulated doxorubicin in living cells," Nanomedicine: Nanotech. Biology Med. **4**, 49–56 (2008).

#105181 - $15.00 USD Received 11 Dec 2008; revised 21 Jan 2009; accepted 21 Jan 2009; published 26 Jan 2009

5. X. W. Dai, M. E. Eccleston, Z. L. Yue, N. K. H. Slater, and C. F. Kaminski, "A spectroscopic study of the self-association and inter-molecular aggregation behaviour of pH-responsive poly(L-lysine iso-phthalamide)," Polymer **47**, 2689–2698 (2006).
6. A. Esposito, T. Tiffert, J. M. A. Mauritz, S. Schlachter, L. H. Bannister, C. F. Kaminski, and V. L. Lew, "FRET Imaging of Hemoglobin Concentration in Plasmodium falciparum-Infected Red Cells," PLoS ONE **3**, e3780 (2008).
7. M. Elangovan, R. N. Day, and A. Periasamy, "Nanosecond fluorescence resonance energy transfer-fluorescence lifetime imaging microscopy to localize the protein interactions in a living cell," J. Microscopy **205**, 3–14 (2002).
8. P. J. Verveer, A. Squire, and P. I. H. Bastiaens, "Global Analysis of fluorescence lifetime imaging microscopy data," Biophys. J. **78**, 2127–2137 (2000).
9. W. Becker, A. Bergmann, M. A. Hink, K. Konig, K. Benndorf, and C. Biskup, "Fluorescence lifetime imaging by time-correlated single photon counting," Micro. Res. Tech. **63**, 58–66 (2004).
10. E. B. van Munster and T. W. J. Gadella, "Fluorescence Lifetime Imaging Microscopy (FLIM)," Adv. Biochem. Engin. / Biotechnology **95**, 143–175 (2005).
11. T. W. J. Gadella, T. M. Jovin, and R. M. Clegg, "Fluorescence lifetime imaging microscopy (FLIM): Spatial resolution of microstructures on the nanosecond time scale," Biophys. Chem. **48**, 221–239 (1993).
12. A. Esposito, H. Gerritsen, and F. Wouters, "Fluorescence lifetime heterogeneity in the frequency domain by lifetime moments analysis," Biophys. J. **89**, 4286–4299 (2005).
13. Q. S. Hanley and A. H. A. Clayton, "AB-plot assisted determination of fluorophore mixtures in a fluorescence lifetime microscope using spectra or quenchers," J. Microscopy **218**, 62–67 (2005).
14. E. Gratton, D. M. Jameson, and R. D. Hall, "Multifrequency phase and modulation fluorometry," Ann. Rev.Biophys. Bioengin. **13**, 105–124 (1984).
15. A. Squire, P. J. Verveer, and P. I. H. Bastiaens, "Multiple frequency fluorescence lifetime imaging microscopy," J. Microscopy **197**, 136–149 (2000).
16. A. D. Elder, S. C. Schlachter, and C. F. Kaminski, "Theoretical investigation of the photon efficiency in frequency-domain FLIM," J. Opt. Soc. Am. A **25**, 452–462 (2008).
17. A. Esposito, H. C. Gerritsen, and F. S. Wouters, "Optimizing frequency-domain fluorescence lifetime sensing for high-throughput applications: photon economy and acquisition speed," J. Opt. Soc. Am. A **24**, 3261–3273 (2007).
18. J. Philip and K. Carlsson, "Theoretical investigation of the signal-to-noise ratio in fluorescence lifetime imaging," J. Opt. Soc. Am. A **20**, 368–379 (2003).
19. A. D. Elder, J. H. Frank, J. Swartling, X. Dai, and C. F. Kaminski, "Calibration of a wide-field frequency-domain fluorescence lifetime microscopy system using light emitting diodes as light sources," J. Microscopy **224**, 166–180 (2006).
20. J. R. Lakowicz, *Principles of fluorescence spectroscopy* (Kluwer Academic, New York, 1999).
21. T. S. Forde and Q. S. Hanley, "Spectrally resolved frequency domain analysis of multi-fluorophore systems undergoing energy transfer," Appl. Spectro. **60**, 1442–1452 (2006).
22. A. H. A. Clayton, Q. S. Hanley, and P. J. Verveer, "Graphical representation and multicomponent analysis of single frequency fluorescence lifetime imaging microscopy data," J. Microscopy **213**, 1–5 (2003).
23. M. A. Digman, V. R. Caiolfa, M. Zamai, and E. Gratton, "The phasor approach to fluorescence lifetime imaging analysis," Biophys. J. **94**, L14–L16 (2007).
24. A. D. Elder, S. M. Matthews, J. Swartling, K. Yunus, J. H. Frank, C. M. Brennan, A. C. Fisher, and C. F. Kaminski, "The application of frequency-domain Fluorescence Lifetime Imaging Microscopy as a quantitative analytical tool for microfluidic devices," Opt. Express **14**, 5456–5467 (2006).
25. Fianium Inc, SC450 datasheet, http://www.fianium.com.
26. E. B. van Munster and T. W. J. Gadella, "Suppression of photobleaching-induced artifacts in frequency-domain FLIM by permutation of the recording order," Cytometry Part A **58A**, 185–194 (2004).
27. J. H. Frank, A. D. Elder, J. Swartling, A. R. Venkitaraman, A. D. Jeyasekharan, and C. F. Kaminski, "A white light confocal microscope for spectrally resolved multidimensional imaging," J Microscopy **227**, 203–215 (2007).
28. E. B. van Munster and T. W. J. Gadella, "phiFLIM: a new method to avoid aliasing in frequency-domain fluorescence lifetime imaging microscopy," J Microscopy **213**, 29–38 (2004).

1. Introduction

FLIM is increasingly important in microscopy because it can be used for the robust quantification of reaction kinetics [2], pH [3], molecular association [4], aggregation [5] molecular proximity [6] and Förster resonance energy transfer [7] among many other parameters. There are several techniques for performing FLIM; here we focus on widefield FD-FLIM, which provides the key benefits of rapid measurement capability and comparatively high photon efficiency.

The majority of FD-FLIM systems are restricted to the measurement of single exponential

#105181 - $15.00 USD Received 11 Dec 2008; revised 21 Jan 2009; accepted 21 Jan 2009; published 26 Jan 2009

lifetime decays. However, monoexponential decays are the exception rather than the rule in biological imaging, as each pixel in the image may contain multiple fluorophores, with different fractional concentrations, and often different local environments. The fluorophore itself may exhibit inherently biexponential fluorescence decays. In this case, an analysis assuming a monoexponential response will be qualitative at best, and often misleading [8]. A simple, robust and efficient method for extending the capability of FD-FLIM systems to measure multiple lifetime components simultaneously is thus a highly desirable objective.

Traditionally, resolving biexponential (or higher) decays has been possible only with Time-Domain FLIM techniques (TD-FLIM) [7] such as Time Correlated Single Photon Counting (TCSPC) [9].

Typical FD-FLIM systems rely on sinusoidally-modulated excitation sources, provided by either acousto-optic modulation of CW sources, or direct modulation of solid state laser sources [10]. The phase shift and modulation change between the sinusoidal excitation and the sinusoidal fluorescence emission is used to determine the lifetime of the fluorophore's exponential decay response [11]. If that response is measured at only one modulation frequency, a biexponential or higher decay cannot be resolved without *a priori* information. Post-processing techniques [8, 12, 13] can extract biexponential parameters from single frequency FD-FLIM data with the prior knowledge that only two spatially invariant, monoexponential lifetimes are present in the image.

This requirement for *a priori* information can be removed by acquiring two or more independent measurements of the fluorophore decay response: N independent measurements allow an N-component lifetime to be resolved. One way of attaining these independent measurements is to vary the excitation modulation frequency. Whilst multi-frequency instruments have long been used for cuvette-based lifetime measurements [14], only one multi-frequency FLIM technique, mfFLIM, has been described in the literature [15]. The mfFLIM technique uses two Acousto-optic Modulators (AOMs) to impose the necessary modulation frequencies onto a CW source.

These AOMs can be dispensed with by using a Dirac excitation source, which provides a train of short (relative to fluorescence decay times) optical pulses. Such a source is inherently composed of many harmonics at integer multiples of the pulse repetition rate. Suitable technology has become widely available in the form of commercial all-fibre based supercontinuum light sources. They feature pulse widths around 10 ps, repetition frequencies on the order of tens of MHz and the benefit of wavelength tuneability over the majority of the visible to near infrared spectrum.

In addition, FD-FLIM with a Dirac excitation waveform has a higher photon economy than FD-FLIM with a sinusoidal excitation waveform. A higher photon economy requires fewer photons to resolve a fluorescence lifetime with a given precision. Several groups have studied photon efficiency for different FLIM techniques, and a figure-of-merit, called the F-value has been devised to provide a quantitative comparison between them. [16, 17, 18]. The F-value is defined as:

$$F = \sqrt{N}\sigma_\tau/\tau \tag{1}$$

where N is the number of photons and σ_τ is the standard deviation of the lifetime τ; hence the best possible F-value is 1 and is obtained when the signal is shot-noise limited. The most common form of FD-FLIM employs a sinusoidal excitation waveform and a square-wave modulated detector gain, and is characterized by an F value of 9. We have shown previously that use of a Dirac pulse train for excitation reduces the F value to 3 [16]. Thus, from Eq. (1), only one ninth as many photons are required to reach a similar precision in the lifetime determination as is the case for sinusoidal excitation.

#105181 - $15.00 USD Received 11 Dec 2008; revised 21 Jan 2009; accepted 21 Jan 2009; published 26 Jan 2009

We report here on the practical implementation of FD-FLIM with a supercontinnuum excitation source which is well represented by the ideal case of a Dirac pulse train excitation waveform. We demonstrate that multiple harmonics can be precisely resolved with the system and apply it for the determination of biexponential fluorescence decays from various samples. In what follows we refer to this technique as multi-harmonic FLIM, mhFLIM. Two algorithms are discussed for analysing mhFLIM data and we validate the technique on well-characterized dyes and in biological samples labeled with spectrally similar fluorophores. The results obtained by mhFLIM are compared with data from TCSPC, and good correspondence is seen between the two techniques.

2. Data processing and theory

In homodyne FD-FLIM, the fluorescent sample is excited by a time-modulated excitation intensity and the emission is imaged using an intensified CCD (ICCD) camera whose optical gain is frequency- and phase-locked to the excitation waveform [10]. The ICCD thus acts as an optical mixer, and the rapid changes in fluorescence emission are sampled by changing the relative phase offset between the ICCD gain waveform and the excitation modulation waveform. A series of images is then acquired with phase offsets varying from 0 to 2π and the signal is averaged over many modulation cycles at each phase step. This permits one to calculate the demodulation and phase delay in the fluorescence emission with respect to the excitation waveform, which in turn allows the fluorescence lifetime of the fluorophore to be determined. In practice, the amplitude and phase response of the FD-FLIM system has to be measured at every frequency used for analysis, and generally such a calibration is performed using a dye sample with a known lifetime [19].

The amplitude and phase response, whether for calibration of the FLIM system or analysis of an unknown fluorophore, are calculated in the same way. A Fourier Transform is taken at each pixel in the series of phase images [10] or, equivalently, a sinusoid is fitted at each pixel [16]. Whether using a Fourier Transform or sinusoidal fitting, a phase and amplitude parameter is extracted for each pixel in the series of images. If the lifetime of the sample is known, these parameters can be used to calibrate the phase and amplitude response of the FLIM system. Once this calibration has been performed, the measured phase and amplitude can be converted into phase and modulation lifetimes for an unknown fluorophore. The sinusoidal fitting approach has the benefit of providing pixel-by-pixel fit-error information with little penalty in processing time (~ 3 s to fit $512 \times 640 \times 36$ pixels on a modern, dual core, PC).

In the case of mhFLIM, phase and amplitude information from several harmonic frequencies in the Fourier Transform is used, rather than only using the fundamental frequency. Likewise, a sum of sinusoids, each having its own phase and amplitude can be fitted at several harmonic frequencies. Thus the mhFLIM system can be calibrated at several frequencies, and the phase and amplitude response of an unknown fluorophore can be measured at several frequencies.

The phase and modulation lifetimes calculated directly from the phase and modulation response have a complicated relationship to the true sample lifetime if there is any heterogeneity in the exponential decay [20, 21]. For this reason, AB-plots (also called phasor plots) that represent FD-FLIM data in an intuitive graphical way are useful [22, 23, 21]. The A and B parameters used to generate the AB plots for each harmonic are extracted from the measured data using sine and cosine transforms:

$$A_n = m_n \sin\theta_n \quad B_n = m_n \cos\theta_n \tag{2}$$

where m_n and θ_n are the modulation and phase respectively of harmonic n. As is evident from these expressions, AB plots are merely a convenient method of representing the amplitude and phase response of the fluorophore in a graphical format. The AB plot also serves to illustrate

#105181 - $15.00 USD Received 11 Dec 2008; revised 21 Jan 2009; accepted 21 Jan 2009; published 26 Jan 2009

the fact that modulation and phase measurements are not independent: for a monoexponential decay, it can be shown that $m_n = \cos(\theta_n)$ and thus all monoexponential responses must lie along a semi-circle in AB space [13, 23] described by:

$$A^2 + (B - 1/2)^2 = 1/4 \tag{3}$$

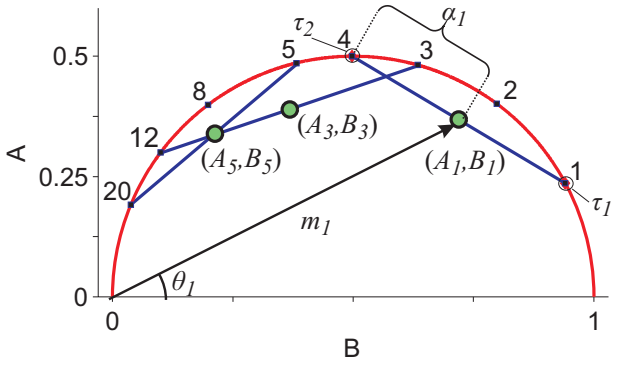

Fig. 1. AB plot showing data for three distinct measurements of a (simulated) biexponential decay sampled at one, three and five times the fundamental frequency of 40 MHz (green circles). Single exponential lifetime components lie on the red semicircle. Numbers on the single-exponential semi-circle indicate decay time in nanoseconds for measurements at the fundamental frequency. See text for further details.

This is illustrated in Fig. 1 by the red semicircle. Points that lie inside the semi-circle have a multi-component decay response. This is shown by the green points in Fig. 1 which refer to a sample containing two fluorophores with lifetimes of $\tau_1 = 4\,\text{ns}$, $\tau_2 = 1\,\text{ns}$ and $\alpha_1 = 0.5$. Here α_1 denotes the fractional contribution of fluorophores with lifetimes τ_1 to the DC fluorescence intensity (note that this is sometimes referred to as f_1 in the literature) [20]). At the fundamental frequency of $\nu_0 = 40\,\text{MHz}$, the resulting biexponential decay is represented by co-ordinates (A_1, B_1) on the AB plot. Data from two further harmonics, measured at $3\nu_0$ (A_3, B_3) and $5\nu_0$ (A_5, B_5) (120 MHz and 200 MHz, respectively) are also shown. The red semicircle in Fig. 1 is labeled with single exponential lifetime values measured at $\nu_0 = 40\,\text{MHz}$. It is seen that components measured at $3\nu_0$ and $5\nu_0$ appear at three and five times the actual lifetime values. For $\tau_1 = 4\,\text{ns}$, corresponding points appear at 12 ns and 20 ns respectively. Lifetime parameters can be converted to AB co-ordinates, assuming a biexponential response, via Eq. (4) and Eq. (5) [8]:

$$A_n(\alpha_1, \tau_1, \tau_2) = \frac{\alpha_1 n\omega_0\tau_1}{1+(n\omega_0\tau_1)^2} + \frac{(1-\alpha_1)n\omega_0\tau_2}{1+(n\omega_0\tau_2)^2} \tag{4}$$

$$B_n(\alpha_1, \tau_1, \tau_2) = \frac{\alpha_1}{1+(n\omega_0\tau_1)^2} + \frac{(1-\alpha_1)}{1+(n\omega_0\tau_2)^2} \tag{5}$$

Here, n refers to the harmonic number, and $\omega_0 = 2\pi\nu_0$ is the fundamental angular frequency of the excitation waveform.

#105181 - $15.00 USD Received 11 Dec 2008; revised 21 Jan 2009; accepted 21 Jan 2009; published 26 Jan 2009

3. Algorithms for resolving heterogeneous decays

3.1. Global Analysis

Collecting data at N harmonics provides N independent equations from which N lifetime components can be resolved. A cost function $C(p)$ can be minimized for every measured harmonic n and at each image pixel p to yield the lifetime components and fractions. In the case of a system containing two lifetime components, τ_1, τ_2 and α_1:

$$C(p) = \sum_{n=1}^{N} \left\{ \left[A_n(\alpha_{1,p}, \tau_{1,p}, \tau_{2,p}) - \hat{A}_n(p)\right]^2 w_n + \left[B_n(\alpha_{1,p}, \tau_{1,p}, \tau_{2,p}) - \hat{B}_n(p)\right]^2 w_n \right\} \quad (6)$$

In the above expression $\hat{A}_n(p)$ and $\hat{B}_n(p)$ are measured quantities. Minimization of $C(p)$ amounts to a multi-frequency global analysis (GA) [8]. Note that in contrast to global analysis applied to single frequency FD-FLIM data, there is no requirement for the lifetimes to be spatially invariant in mhFLIM. In biological samples this is useful, because spatial heterogeneities (eg. variations of pH, molecular association, etc.) can locally affect lifetimes. Eq. (6) allows such information to be retrieved from the data: not only can the fractions of the fluorescing entities be recovered but also the spatial variation of the individual lifetime components. Of course, it is also possible to analyze mhFLIM data on the assumption of spatial invariance of the lifetime. Whilst this may lead to loss of information, the advantage lies in the greatly improved the signal-to-noise ratio (SNR) of the measurement.

Eq. (6) includes weighting factors w_n to account for the decreasing fidelity of data collected at higher harmonics as the modulation depth decreases with n. Thus data with lower SNR (high n) are weighted less strongly than data from lower harmonic frequencies. The weighting factors were experimentally determined at each harmonic by measuring the standard deviation of the A and B parameters obtained from well characterized dye samples; w_n is then defined as the ratio of the variance of harmonic n to that of the first harmonic, i.e.: $w_n = \sigma(A_1)/\sigma(A_n)$. The weighting factors measured ($w_1 = 1$, $w_3 = 0.36$, $w_5 = 0.21$) closely match the amplitude weightings for the first three (odd) Fourier components of a square wave ($w_1 = 1$, $w_3 = 0.33$, $w_5 = 0.20$). This is a manifestation of decreasing modulation depth as the major cause for the decreasing SNR with harmonic number.

3.2. Weber algorithm

A closed-form analytical method to extract multi-component lifetime data from multi-harmonic measurements was derived by Weber and is reported in [1]. The method permits moments of lifetime distributions to be evaluated analytically from AB parameters obtained at several harmonic frequencies. Because no non-linear minimisation is required, the computation of lifetime parameters is much faster compared to the method described above. Weber showed that a measurement involving N harmonics permits $2N-1$ moments to be evaluated, which, in turn, permit the resolution of N lifetime components from the measurement sample. For a system containing just two lifetime components the algorithm reduces to the following two equations:

$$M_0 = h_1^2 B_1 - h_2^2 B_2 \quad M_1 = h_1 A_1 - h_2 A_2 \quad (7)$$

$$M_2 = -B_1 + B_2 \quad M_3 = A_1/h_1 + A_2/h_2 \quad (8)$$

where h_r is the harmonic number (i.e.: $h_1 = 1$, $h_2 = 3$) and M_k is the moment of order k. The individual components of a biexponential decay can then be determined from (note that Eq. (35) in [1] is missing parentheses, and Eq. (32) is missing a subscript):

#105181 - $15.00 USD Received 11 Dec 2008; revised 21 Jan 2009; accepted 21 Jan 2009; published 26 Jan 2009

$$\theta_1 = (M_3M_0 - M_2M_1)/(M_2M_0 - M_1) \quad \theta_2 = (M_3M_1 - M_2)/(M_2M_0 - M_1) \tag{9}$$

$$\tau_1, \tau_2 = \left[\theta_1/2 \pm (\theta_1^2/4 - \theta_2)^{1/2}\right]/\omega \tag{10}$$

$$\alpha_1 = 1 - \frac{B_1 - \left(1 + h_1^2\tau_1^2\right)^{-1}}{\left(1 + h_1^2\tau_2^2\right)^{-1} - \left(1 + h_1^2\tau_1^2\right)^{-1}} \tag{11}$$

The two lifetimes and their amplitude fractions can thus be computed in every image pixel from mhFLIM data on application of Eqs. 7 - 11. Since they are closed-form expressions, this computation is orders of magnitude faster than other techniques (< 1 s to process 256×256 pixels, see Table 1). In theory, more than two harmonics could be used to resolve more than two lifetime components, but because the SNR is rapidly decaying with harmonic number, this is only useful for samples with high SNR.

4. Materials and methods

Fig. 2 shows a schematic overview of the mhFLIM set-up developed. The instrument consists of an Olympus IX50 inverted wide-field microscope frame and a modified version of a commercial FD-FLIM system described previously [24].

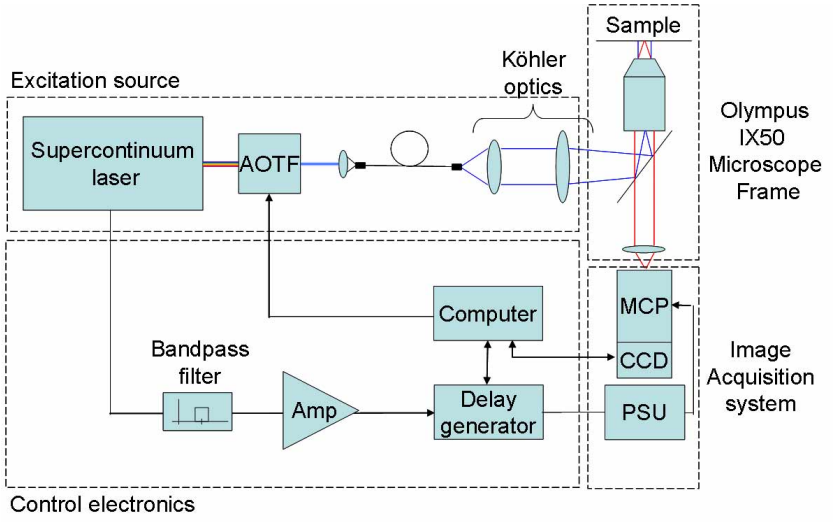

Fig. 2. Overview of the mhFLIM instrument. MCP = Multi-Channel Plate, CCD = charge coupled device array, PSU = power supply unit, AOTF = Acousto-Optic Tunable Filter.

4.1. Supercontinuum source

A white light supercontinuum source (SC450, Fianium Inc.) was used to provide the excitation wave train. The source emits light from 450 nm to 2000 nm at a power spectral density of greater than $1\,\mathrm{mW/nm}$ across the spectrum. The pulse repetition rate of the source was around 40 MHz with pulse widths on the order of tens of picoseconds [25]. Compared with the lifetimes of typical biological fluorophores (hundreds of ps to several ns), the excitation waveform is well represented by a Dirac pulse train. An acousto optic tunable filter, AOTF (AOTFnc-vis,

#105181 - $15.00 USD Received 11 Dec 2008; revised 21 Jan 2009; accepted 21 Jan 2009; published 26 Jan 2009

AA Optoelectronique, France), was used as a frequency selective tuneable filter. 1 nm wide portions of the spectrum were selectable between 450nm and 700nm, and the light was focused onto the back focal plane of the microscope objective to provide Köhler illumination.

4.2. Image intensifier

A lens coupled image intensifier (II18MD, Lambert Instruments, Netherlands) was gain modulated at the pulse repetition rate of the supercontinuum source. The gain modulation waveform was derived directly from the output signal of a pulse monitoring photodiode in the supercontinuum source to ensure that the gain modulation frequency was identical to the pulse repetition rate. The photodiode signal was passed through a variable delay generator with 20 ps precision (Kentech Instruments). Its output was subsequently amplified (Stanford Research Systems, SR445A) and low pass filtered to produce a sinusoidal waveform at the laser repetition frequency. This yielded a signal with an amplitude of 6V peak-to-peak, which was applied to the photocathode of the intensifier together with a DC offset voltage of $-1.4\,\mathrm{V}$.

Measurements of the DC gain characteristics of the image intensifier are presented in Fig. 3(a). It is evident that the ICCD gain has a highly nonlinear response to the photocathode voltage. Essentially, the device operates either in an 'on' or 'off' state with a sharp transition at around $-2\,\mathrm{V}$.

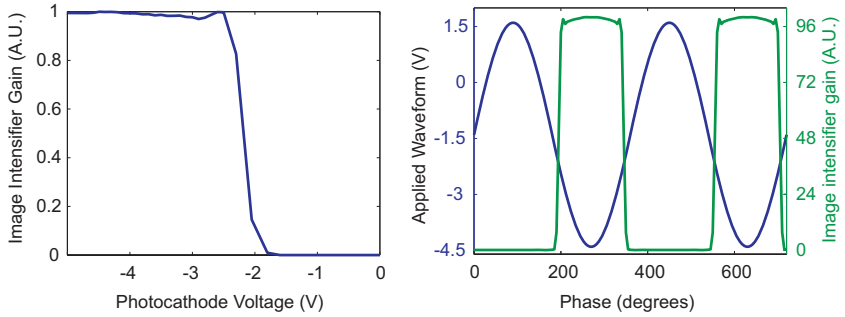

Fig. 3. (A) DC response of image intensifier gain vs. photocathode voltage. (B) (simulation) The sinusoid shown in blue applied to the measured photocathode DC response (shown in (A)) produces the image intensifier gain profile show in green.

The application of a sinusoidal waveform to the photocathode produces an ICCD gain that is essentially a square wave with its fundamental frequency locked to the repetition rate of the excitation light (see Fig. 3(b)). The Fourier Transform of a typical experimental gain waveform (measured using reflection from a glass coverslip [15]) is shown in Fig. 4. Approximately 15 harmonics of the fundamental frequency are detected, and, as expected for a square waveform, only odd harmonics carry significant amplitude.

4.3. Calibration of the ICCD

For quantitative fluorescence lifetime measurements, it is important to correct for the inherent phase delays in the ICCD electronics as well as spatial variations in the response of the ICCD. Reference measurements were made on dye samples with known lifetimes to calibrate the image intensifier. The results of such a calibration are presented in Fig. 5. A $10\,\mu\mathrm{M}$ solution of Rose Bengal in ethanol (Sigma Aldrich, Inc) was used as a reference sample. This dye features a monoexponential decay with a lifetime of 780 ps (measured with TCSPC). The phase response of the image intensifier, θ^n_{ICCD}, was calculated at harmonic n using the formula

#105181 - $15.00 USD Received 11 Dec 2008; revised 21 Jan 2009; accepted 21 Jan 2009; published 26 Jan 2009

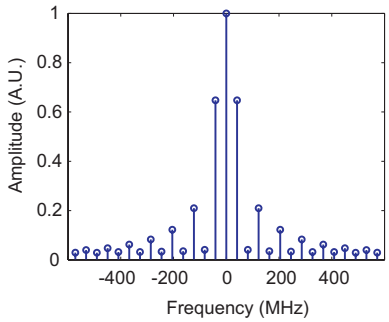

Fig. 4. Fourier transform of a measured ICCD gain waveform.

$\theta^n_{ICCD} = \theta_{n,ref} - \tan^{-1}(-1/n\omega_0\tau_{ref})$ [16]. The maximum phase delay across the intensifier increased from 5.7° at the first harmonic to 26° at the fifth harmonic. Moreover, the mean phase delay increased approximately linearly from the fundamental frequency to the 5th harmonic. An equivalent set of calibration images was also generated for the amplitude response of the ICCD, using $m^n_{ICCD} = \{m_{n,ref}[1+(n\omega_0\tau_{ref})^2]^{1/2}\}^{-1}$.

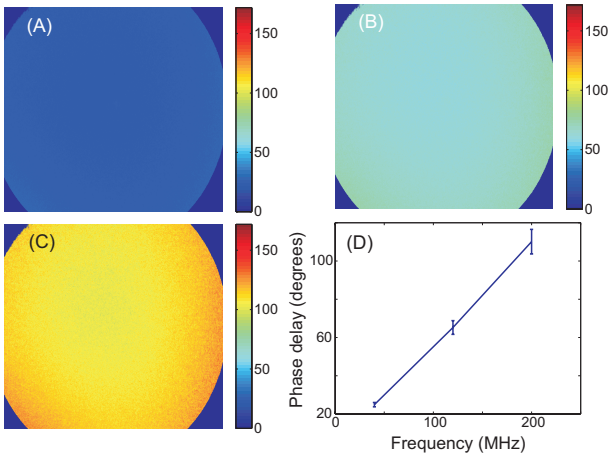

Fig. 5. Phase variation across the ICCD at the fundamental frequency of $\nu_0 = 40$ MHz (A), the third harmonic of $3\nu_0 = 120$ MHz (B) and the $5\nu_0 = 200$ MHz. (D) The mean phase delay versus frequency; error bars indicate the standard deviation. The data were obtained from a calibration with Rose Bengal dye.

4.4. Biological sample preparation

Human neuroblastoma (SH-SY5Y) cells were grown in Minimal Essential Medium plus 15% foetal calf serum, 1% Non Essential Amino Acids, 2mM N-glutamine and 1% Penicillin-Streptomycin (Sigma, UK). 1×10^6 cells were plated onto Matek cell culture dishes and cultured at 37°C and 5% CO_2. After 24 h, the cells were washed 3× with ice-cold phosphate buffered saline (PBS; pH 7.4) before fixing them with ice-cold 4% paraformaldehyde in 0.1 M phosphate buffer (pH 7.4) for 10 min at room temperature (RT). After fixation, the cells were washed 3× with PBS before incubating them with either 5% normal goat serum (NGS) or 5% normal donkey serum (NDS) and 0.25% Triton X-100 in PBS for 1h at RT. Thereafter the cells were incubated with either anti-human laminin IgG (1:1000) (Abcam, Cambridge,UK), or

#105181 - $15.00 USD Received 11 Dec 2008; revised 21 Jan 2009; accepted 21 Jan 2009; published 26 Jan 2009

anti-human Map2 IgG (1:500) (Chemicon, CA, USA) with 5% NGS or NDS, respectively, and 0.25% Triton X-100 in PBS overnight at RT. The cells were rinsed 3× with PBS and incubated with secondary goat anti rabbit antibody labeled with Alexa 546 (1:200) and donkey anti mouse antibody labeled with Alexa 555 (1:100; both Invitrogen, UK), 2% NGS or NDS respectively, 0.25% Triton X-100 in PBS for 1h in the dark at RT. Thereafter the cells were rinsed again 3× with PBS before imaging.

4.5. Image acquisition

All data presented in this paper (mhFLIM and TCSPC) were acquired using a 100x objective (NA=1.40, Olympus Inc.). Theoretically, only eleven phase steps are required to resolve five harmonics. In practice, more are needed to prevent artifacts due to frequency aliasing. For all experiments reported here, 36 equally spaced phase steps were used during image acquisition to cover a full modulation period. Signals were integrated for 100 ms at each phase step. The phase steps were not temporally ordered and a pseudo-random phase sequence was used, a method that has been shown to reduce artifacts induced by photobleaching in FD-FLIM [26]. The same pseudo-random phase sequence was used for all measurements. Excitation was at 553 nm, and emission was collected through a longpass emission filter transmitting above 590nm. A 3×3 pixel bin was applied to all mhFLIM data.

For validation, all sample lifetimes were also measured using a TCSPC FLIM system (SPC-830 Becker and Hickl, Germany). The supercontinuum source described above was used for excitation in a custom-built confocal scanning microscope, details of which are given in [27]. The excitation and emission parameters were the same as those used for the mhFLIM measurements. Photon count rates were kept below 1% of the laser repetition rate to prevent pulse pile-up. Images were acquired for 100 s, and photobleaching was negligible. All TCSPC images were subsequently processed using SPCImage (Becker and Hickl, Inc) and fit with a bi-exponential decay function. Pixel binning was increased until approximately 15,000 to 25,000 photons were obtained per pixel.

5. Results

5.1. Dye solutions

The mhFLIM system was tested using solutions with uniform concentrations of organic dyes. In the first test, a drop of Rhodamine 6G dye in ethanol at $25\,\mu$M concentration was imaged. Fig. 6 shows a phasor plot of the fluorescence lifetime measurements at the fundamental frequency (~ 40 MHz) as well as at the third and fifth harmonics. Close to the 4 ns mark on the semicircle representing monoexponential decays one recognises a cluster of pixels, corresponding to the fundamental measurement frequency. Further clusters are seen to lie close to 12 and 20 ns, corresponding to measurements from $3\nu_0$ and $5\nu_0$, respectively. The experiment was repeated with Rose Bengal ($10\,\mu$M in ethanol), and a monoexponential decay of 760 ps was measured, which is in good agreement with TCSPC (see Table 1). A monoexponential response was also measured at $3\nu_0$ and $5\nu_0$. Though mhFLIM acquired the lifetime images more than 20× faster than TCSPC, the SNR achieved by each method is similar (see Table 2; standard deviations were calculated on a 256×256 pixel ensemble). This speed increase stems from the fact that mhFLIM does not require reduced photon rates to avoid pulse pile up, as is the case for TCSPC.

The Rhodamine 6G and Rose Bengal solutions were then mixed in equal parts and imaged under identical conditions. The results are shown in Fig. 6(c). Clearly, the AB cluster has now moved inside of the semicircle, indicative of a multicomponent decay response.

The lifetime components of the mixture were estimated using the global analysis algorithm, Eq. (6), which was applied to the mean of the pixel ensemble (because the lifetime is spatially

#105181 - $15.00 USD Received 11 Dec 2008; revised 21 Jan 2009; accepted 21 Jan 2009; published 26 Jan 2009

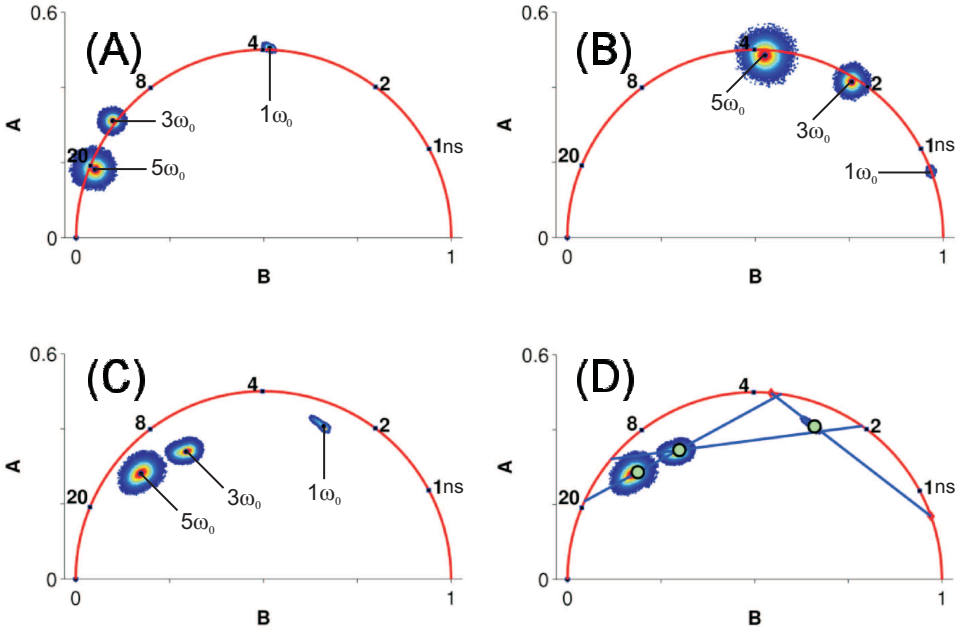

Fig. 6. Phasor plots from mhFLIM measurements at $1\nu_0$, $3\nu_0$, and $5\nu_0$ for (A) Rhodamine 6G in ethanol. (B) Rose Bengal in ethanol. (C) Rhodamine 6G and Rose Bengal mixture in ethanol. (D) The same dye mixture shown with a biexponential estimate from Eq. (6). The numbers along the semicircle indicate the single-exponential lifetimes for measurements at the fundamental frequency.

Table 1. Processing times for a 256×256 pixel image.

Technique	**Processing time**
GA mhFLIM	4400 s
TCSPC	400 s
Weber mhFLIM	< 1 s

invariant in this mixture). The result ($\tau_1 = 0.74$ ns, $\tau_2 = 3.8$ ns and $\alpha_1 = 0.29$) is in good agreement with expectations. The data and results from the fit are shown in Fig 6(D), with the three straight lines corresponding to ν_0, $3\nu_0$, and $5\nu_0$.

Fig. 7 shows a comparison of data analysed with mhFLIM using global analysis (blue) and the Weber algorithm (green) presented in Eq. (7) - Eq. (11). Data from TCSPC is also presented (red lines). As noted earlier, the Weber algorithm uses only two harmonics for resolving biexponential decays, and this partly explains the larger standard deviations on the obtained distributions. However, good agreement is achieved between all three methods for both lifetime values.

5.2. Biological samples

Experiments were carried out on cells labelled with spectrally similar dyes. SH-SY5 cells were prepared as described in Section 4.4 and labelled with Alexa 555 and 546. Corresponding mhFLIM data from the cells are presented in Fig. 8. The position of data clusters within the semi-

#105181 - $15.00 USD Received 11 Dec 2008; revised 21 Jan 2009; accepted 21 Jan 2009; published 26 Jan 2009

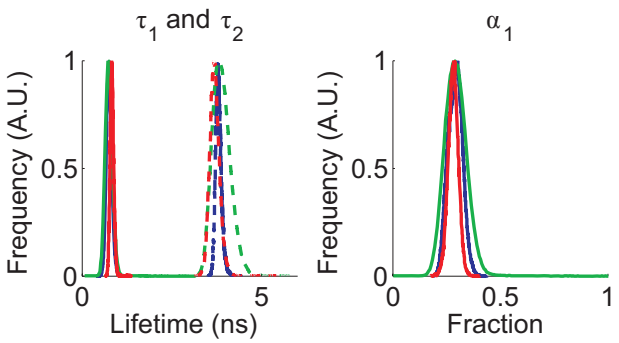

Fig. 7. Peak-normalized histograms showing lifetime components of Rhodamine 6G and Rose Bengal mixture in ethanol using TCSPC (red), mhFLIM with global analysis (blue) and mhFLIM with Weber algorithm (green)

Table 2. Lifetimes of pure dye samples calculated using different techniques (ns).

Technique	**Rhodamine 6G**		**Rose bengal**	
	Mean	Std Dev	Mean	Std Dev
TCSPC	3.83	0.16	0.76	0.05
GA mhFLIM	3.82	0.17	0.75	0.09
Weber mhFLIM	3.75	0.42	0.83	0.15

circle clearly indicates the presence of multicomponent lifetimes. Lifetime component images of the cells are shown in Fig. 9(a). Results are shown for TCSPC, mhFLIM using the global analysis algorithm, and mhFLIM using the Weber algorithm. Histograms for the three methods are shown in Fig. 9(b). Good agreement is observed for results obtained via the two mhFLIM algorithms (GA and Weber) in both the lifetime values and the fractions. Agreement for τ_1 and τ_2 is also excellent between the TCSPC and mhFLIM results. The apparent difference in α_1 observed between TCSPC and mhFLIM stems from the fact that it was not possible to image the same set of cells when switching between the confocal (TCSPC) and widefield (mhFLIM) systems and thus the difference reflects the variation of dye components between different sets of cells.

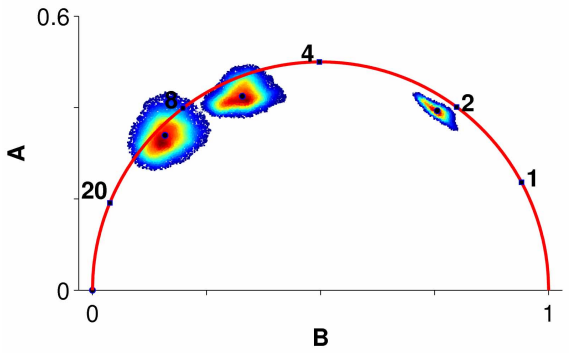

Fig. 8. AB plot showing mhFLIM data from SH-SY5 cells labeled with Alexa 555 and Alexa 546 dyes.

#105181 - $15.00 USD Received 11 Dec 2008; revised 21 Jan 2009; accepted 21 Jan 2009; published 26 Jan 2009

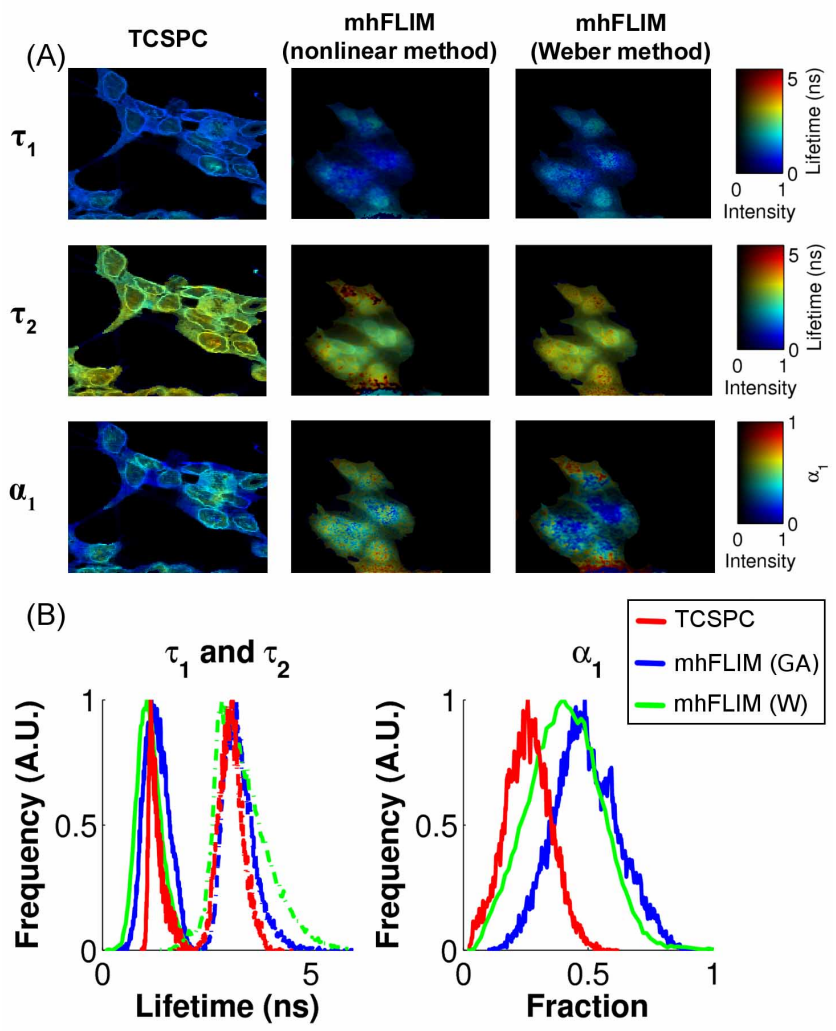

Fig. 9. (A) Lifetime components derived from TCSPC, mhFLIM processed with GA algorithm and mhFLIM processed with Weber algorithm. The mean lifetime, τ_m is derived from $\tau_m = \alpha_1\tau_1 + (1-\alpha_1)\tau_2$. TCSPC images are approximately $140\,\mu$m $\times$ $140\,\mu$m and mhFLIM images are $100\,\mu$m $\times$ $100\,\mu$m(B) Peak-normalized histograms of the data shown in (A). TCSPC data is shown in red, mhFLIM processed with GA algorithm in blue and mhFLIM processed with the Weber algorithm in green.

6. Conclusion

We have demonstrated that biexponential fluorescence decays can be resolved using wide-field frequency-domain FLIM with a supercontinuum light source for excitation. In particular, using a source pulsed at ν_0 of around 40 MHz permitted useful information to be retrieved from higher harmonics up to five times the fundamental frequency. The square wave gain profile of the image intensifier suppresses even harmonics in the signal waveform, but significant amplitudes at ν_0, $3\nu_0$ and $5\nu_0$ means that in principle up to three lifetime components can be fitted simultaneously.

#105181 - $15.00 USD Received 11 Dec 2008; revised 21 Jan 2009; accepted 21 Jan 2009; published 26 Jan 2009

We demonstrated the technique, which we term mhFLIM on samples exhibiting two exponential decay components, a feature of many important fluorescent labels used in biological microscopy. We validated and compared mhFLIM data with TCSPC measurements and found good agreement. We demonstrated the use of two algorithms for extracting biexponential decays from multi-harmonic data. A global analysis algorithm was implemented which yields accurate lifetime data but is computationally costly because of the non-linear minimisation routine employed. A much faster algorithm, originally developed by Weber [1] was also tested, which analytically generates moments of the lifetime distribution from multi-harmonic data, and thus features greatly increased execution speed.

A speed limitation of the technique, as implemented in its current form, is caused by the large number of harmonic frequencies present in the signal waveform due to the square wave detector gain profile. Although much reduced in amplitude, frequencies $> 5\nu$ cannot be ignored and these cause aliasing artifacts unless the data are significantly oversampled. Theoretically, eleven phase steps should suffice to resolve the three harmonic components $(1, 3, 5\nu_0)$, but in practice 36 phase steps were needed to obtain reasonable precision.

These aliasing effects can perhaps be mitigated through use of a modified ϕ FLIM [28] approach that preserves some of the harmonics or by modulating the MCP voltage rather than the photocathode voltage, with the objective of producing a smoother gain waveform with fewer harmonics.

mhFLIM is readily implemented in existing wide-field FD-FLIM systems. The main requirements are a fast-response image intensifier and an excitation source with relatively short pulses at tens of MHZ repetition rates, for which photonic crystal fibre generated supercontinuum sources are ideally suited. Their great wavelength flexibility, compact size and high output power make them useful for confocal applications [27] and also widefield microscopy.

Acknowledgments

This work was supported by grants from the BBSRC (grant BB/F016336/1) and the EPSRC (grant EP/F028261/1). J.H. Frank acknowledges support from the U.S.A. Department of Energy, Office of Basic Energy Sciences, Division of Chemical Sciences, Geosciences, and Biosciences.

#105181 - $15.00 USD Received 11 Dec 2008; revised 21 Jan 2009; accepted 21 Jan 2009; published 26 Jan 2009